Nonlinear Modeling and Identification of a DC-Motor with Friction and Cogging

Steffen Buechner*, Viktor Schreiber†, Arvid Amthor*, Christoph Ament* and Mike Eichhorn‡

*Institute of Automation and Systems Engineering
Ilmenau University of Technology, Ilmenau, 98693, Germany
Email: steffen.buechner@tu-ilmenau.de
†Department of Automotive Engineering
Ilmenau University of Technology, Ilmenau, 98693, Germany
‡IAV GmbH - Ingenieurgesellschaft Auto und Verkehr, Gifhorn, 38518, Germany

***Abstract*—In the presented work a nonlinear, analytic model of a permanent magnet direct current motors with brushes is proposed. Besides the theoretical modeling an automated identification algorithm for this detailed model is deduced. The resulting model includes the electromechanic and electromagnetic effects of the direct current machine, like voltage induction or motor torque, and additional nonlinear phenomena. These nonlinearities include cogging torque, eddy current, hysteresis losses and tribological aspects. The cogging torque is caused by a variation of the magnetic flux density, which manifests itself as a periodic oscillation in the torque curve. In addition, eddy current and hysteresis losses arise by the commutation of the magnetic field in the armature, are also captured by the motor model. The tribological aspects of all friction regimes are modeled utilizing the elasto-plastic friction model. This model can reflect the linear spring damper behavior of the elastic friction domain as well as velocity depending friction behavior of the plastic friction domain. The parameters are separately identified through specific experiments referring to their physical equivalents. Therefore, two testing benches are developed in order to capture the different effects in the direct current motor.**

I. Introduction

To remain competitive in the global market, vehicle components must be optimized to their application to increasing environmental awareness and comfort aspects. Therefore, the component itself has to be designed perfectly and also its excitation has to be adapted. This requires detailed knowledge about structure, functionality and system behavior. To maximize the set goals and shorten the time of development models of vehicle components are indispensable. The benefit of such physically motivated models reaches from component design over system simulations till optimized controller design. Modern vehicles contain a rising number of electromechanically actuators driven by brushed DC-motors. To increase the efficiency of such motors and their control systems an accurate system model for DC-motors is essentially.

Hence, the motivation of this publication is the detailed modeling of a permanent magnet DC motor that can rebuild all essential electromechanical and electromagnetic phenomena. From the field of literature, [1] offers a good overview of the physical processes of electrical machines. Besides the well-known phenomena such as inertia and the equivalence between torque and current, the friction is often modeled as linear function (see for example [2], [3], [4]). Due to the highly nonlinear characteristic of friction, this causes problems especially at precise positioning tasks [5], [6].

To improve this, the proposed motor model will be extended by a dynamic friction model, the so called elasto-plastic friction model [7], which is adapted for rotary systems [8]. It is an extension of the Lund-Grenoble model [9] and can simulate most of the major nonlinear friction phenomena like presliding displacement, the Stribeck effect, frictional lag, stick-slip motion and many more, which are proposed in [10].

Another essential component of the presented model is the cogging torque. This behavior is investigated by using FEM simulations based on geometric data shown in [11], [12] and shows that the qualitative shape of the cogging torque can be approximated as a periodic function depending on the angular position. Considering the electromagnetic effects, as known in the literature (e.g. [4], [11]), often modeled without iron losses produced by eddy current and hysteresis losses [4]. Since the magnetic quantities can be measured only under difficult conditions, this paper presents a way to ascribe the iron losses to the motor current and velocity.

In addition to this an adapted identification algorithm of the model parameters is presented. In literature many identification algorithms are proposed based on step response [2]. This means that the used model has to be linear or has to be linearized like in [3] or [4]. In this papers all parameters are identified in separate, specialized experiments to reduce mismatch of the parameters to reality.

Section II presents the experimental set-up of this identification. After explaining the model in detail, the identification algorithm for the different model parameters will be introduced in section IV. Before drawing conclusions, experimental results in section V demonstrate the effectiveness of the proposed approach.

978-1-4799-0224-8/13/$31.00 ©2013 IEEE

II. Experimental Set-Up

For identification of the DC-motor behavior two test beds are developed. This is absolutely necessary, because for identification a huge range of torques as well as angular velocities (in respect to the needed resolution) have to be realized. In both test beds the target, in this case the DC-motor, the sensor system and the actuator are arranged aligned with the rotatory axis. All actuators are driven by proprietary developed analog current amplifiers with an extraordinary high precision. The dynamical behavior of the amplifier and the motor can be neglected due to the fact that the overall cut-off-frequency is higher than 10 kHz. In this case, the motor torque $M(t)$ is proportional to the output of the amplifier, the current $i(t)$.

$$M(t) = k_A \cdot i(t) \tag{1}$$

The test motor shall not be destroyed for identification the test motor. So the measured variables are restricted to the rotation φ, the torque M, the voltage u and the motor current i. Values like magnetic flux B are not measured. For data acquisition and control, a modular dSpace real-time system [13] in combination with Matlab/Simulink® is utilized.

A. Motor test bed

The motor test bed can be seen in Figure 1. It consists of (from left to right) the analyzed DC-motor, a rotary sensor, a shaft fixing to optional rotation lock, a torque sensor and the test bed actuator. Nearest to the motor is an analogue, incremental rotary encoder, constructed by the company Heidenhain for angle measurements with a resolution of 0.7 μrad [14], mounted. This construction reduces measurement errors, which are induced by torsion. Second part of the sensor system is a dual range torque sensor made by Kistler [15]. This is used to realize optimal torque measurement for different sizes of motors. Last part of the presented experimental set-up is an ironless DC-motor, which actuates the system.

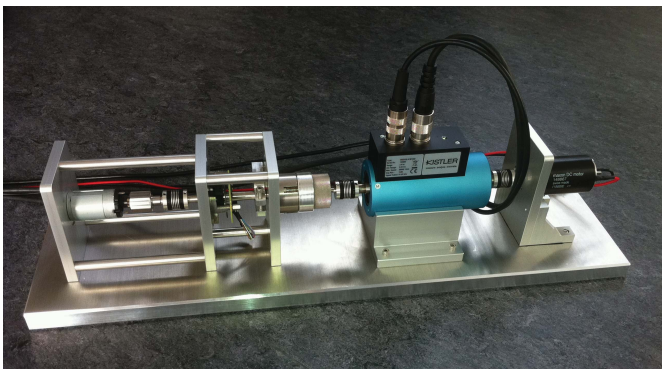

Fig. 1. Test Bed for Motor Identification

B. Friction Test Bed

As shown in Figure 2, the DC-motor, the sensor system as well as the voice coil actuator are arranged aligned vertical to reduce errors by unbalance. At the bottom the DC-motor with its bearings can be found.

Located above is an analogue, high-resolution, incremental rotary encoder, made by Heidenhain and works with a resolution of 0.3 μrad [14]. A rotary voice coil motor driven by a current amplifier actuates the system. There is no torque measurement in this system because available torque sensors lacking accuracy. The torque will be inferred from the current. Advantage of this setup, is to realize and measure arbitrary small torques only depending on the variable gain of the current amplifier. However the limited moving range is a drawback but this do not affects the identification of frictional behavior that much.

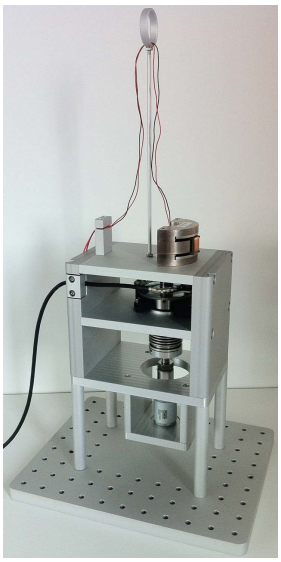

Fig. 2. Test bed for friction identification

III. Motor Model

The developed model for a direct current motor with brushes can be separated in two parts. First part is the electromagnetic part, which contains all voltage generating effects. In the second part all torque generating parts are summarized in the electromechanic model.

A. Electromagnetic Model

The electromagnetic model reproduces the voltage drop of different components (see equation (2)).

$$u = u_{\mathrm{R}} - e_\sigma - e_\delta + u_{\mathrm{EC}} + u_{\mathrm{Hys}} \tag{2}$$

For this armature voltage u consists of classical components like voltage drop of the ohmic resistance u_{R}, leakage reactance of the coil inductances e_σ, induction voltage generated by rotor movement e_δ and is extended by voltage loss caused by eddy currents u_{EC} and magnetic hysteresis u_{Hys}. The ohmic voltage drop is expressed by the motor current i with $u_{\mathrm{R}} = Ri$, where R includes all ohmic resistances from coil, collector and connectors. In the same way leakage reactance is defined by current change $\dot{i}$ with $e_\sigma = -L\dot{i}$. Last classical part is the induction voltage $e_\sigma = -k_{\mathrm{b}}\dot{\varphi}$, which depends on the rotation velocity.

1) Eddy Current: Due to rotation and commutation the magnetization of the rotor field changes. This induces a voltage in the coil as well as in the iron core of the rotor and result in the so called eddy currents in the iron core (see Figure 3).

These currents produce heat and power loss and so there are many constructive approaches to minimize these losses, like division and isolation of the iron core. Nevertheless it cannot be eliminated and hence have to be modeled.

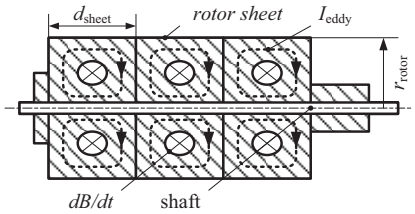

Fig. 3. Eddy current

$$E_{\text{EC}}(y) = \frac{\mathrm{d}B}{\mathrm{d}t} y \tag{3}$$

Based on the electric field (equation (3)), the conductance and the geometry of the iron core the power loss can be modeled as follows:

$$u_{\text{EC}} = \frac{d_{\text{sheet}}^2}{24} \kappa_{\text{fe}} V_{\text{fe}} \dot{\varphi}^2 B^2 \frac{1}{i} \overset{B \sim i}{\Longrightarrow} u_{\text{EC}} = k_{\text{EC}} \dot{\varphi}^2 i \tag{4}$$

In the presented work one goal is to not destroy the motor for identification, so it is not possible to measure magnetic flux B. Under the assumption that the magnetic flux B is proportional to the motor current i it can be replaced with an additional proportional factor. This proportional factor and also the geometric parameters like sheet strength d_{sheet} are unknown and therefore they are lumped to one new parameter k_{EC} (see equation (4)).

2) Hysteresis: One significant characteristic of iron is its hysteresis effect, when changing the magnetization. The size and shape is different for magnetically soft or hard materials (see Figure 4).

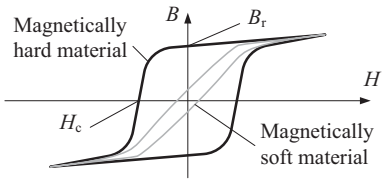

Fig. 4. Magnetization curve

The enclosed area of the magnetization curve defines the specific work w_{Hys} for changing the magnetization (see equation (5)).

$$w_{\text{Hys}} = \oint H \mathrm{d}B \tag{5}$$

As already mentioned the motor should not be destroyed and hence the magnetic flux B is not measureable. Also many material dependent parameters are unknown and therefore they are concentrated in one new parameter k_{Hys} (see equation (6)).

$$u_{\text{Hys}} = \tilde{k}_{\text{Hys}} V_{\text{fe}} f B^2 \frac{1}{i} \overset{B \sim i, f \sim \dot{\varphi}}{\Longrightarrow} u_{\text{Hys}} = k_{\text{Hys}} \dot{\varphi} i \tag{6}$$

B. Electromechanic Model

The electromechanic model contains the different torques generated by the motor itself and external influences like described in equation (7).

$$M_{\text{Mot}} = k_{\text{t}} i = J_{\text{m}} \ddot{\varphi} + M_{\text{L}} + M_{\text{Cog}} + M_{\text{F}} \tag{7}$$

Like in simple motor models the motor torque M_{Mot} is generated by motor current i and the torque-forming constant k_{t}. This torque is used to accelerate the rotor mass with its rotatory inertia J and perform mechanical work on the load torque M_{L}. Additional components in this model are the nonlinear cogging M_{Cog} and friction torques M_{F}, which are defined below.

1) Cogging Torque: The cogging torque is caused by the air-gap permeance variation due to slotting effect which is typically independent of the motor current i. The exciter field collapses with a period of N in account to the angle of the stator Γ, where N is the number of slottings in the rotor (see Figure 5).

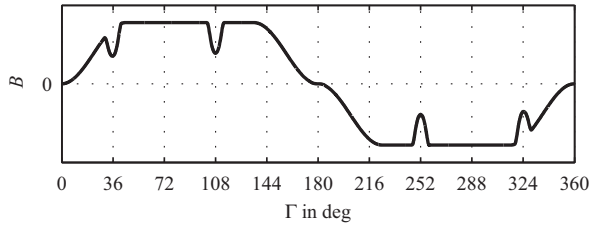

Fig. 5. Exciter field under influence of rotor slotting

By moving the rotor, the slotting caused collapses change their position in the exciter field. This causes variations in the exciter field and also in the magnetic work W_{Mag}. With:

$$M_{\text{Cog}} = \frac{\partial W_{\text{Mag}}}{\partial \varphi} \tag{8}$$

It can be seen, that also the cogging torque M_{Cog} changes over rotor position. A simulating of these effects results in a periodic oscillating cogging torque with a period depending on geometric parameters (see Figure 6).

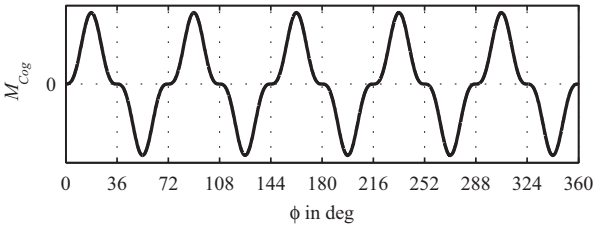

Fig. 6. Cogging torque over rotor position

With this information cogging torque could be calculated using the following:

$$M_{\text{Cog}} = \hat{M}_{\text{Cog}} f(\varphi) \tag{9}$$

2) Friction Torque: To rebuild the friction torque of a DC-motor the elasto-plastic friction model is used, which was introduced by Dupont *et al.* [7]. This model can reflect elastic, plastic and transition domain separately. The model is based on the assumption that the surfaces of two rubbing objects consist of small bristles which interact to each other. For simplification only one side of the interacting surfaces has elastic bristles (see Figure 7) and all deflections are reduced to a mean deflection of all bristles z.

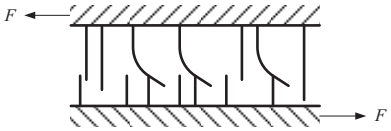

Fig. 7. Bristle model

The movement of a body can be elastic, elasto-plastic or plastic. In case of small force F, the bristles will be deflected and if the force is reduced, the moving object returns to the initial position (elastic displacement). In case of higher forces, the deflection of the bristles exceeds the critical value and the movement consists of an elastic as well as a plastic component (elasto-plastic domain). If the force is high enough to exceed the maximal deflection, the bristles slide upon one another and a plastic displacement occurs. As the motor is a rotary system all displacements are angular displacements and all forces are torques. This torque is defined like follows:

$$M_{\mathrm{F}} = \sigma_0 z + \sigma_1 \dot{z} + \sigma_2 \dot{\varphi} \tag{10}$$

The friction is characterized by a stiffness σ_0 and a damping coefficient σ_1. Where the bristle deflection z is modeled like this:

$$\dot{z} = \dot{\varphi}\left(1 - \alpha \frac{z}{z_{\mathrm{ss}}}\right) \tag{11}$$

This steady state deflection z_{ss} defines the maximum friction torque, which is known as Stribeck curve.

IV. Identification Process

In common with the modeling, identification is separated by the present effects of the DC-motor. Division of the whole highly nonlinear system behavior results in manageable parts. For each effect an optimal identification experiment was designed to get an excellent fit of parameters to their physical equivalents. The determination of only significant parameters for each experiment reduces the mismatch of parameters and increases model quality.

A. Electromagnetic Model

All identification sequences for the electromagnetic model are realized using the motor test bed.

1) Ohmic resisitance and leakage inductance: The ohmic resistance and the leakage inductance will be identified utilizing the same experiment, because both depend only on motor voltage u and motor current i or current derivative $\dot{i}$. Hence resistance effects can be separated from inductance effects. For the experiments the motor position was locked by position control of the test bed motor. Under this conditions motor velocity $\dot{\varphi}$ equals zero and the electromagnetic model equation (2) can be reduced to:

$$u = Ri + L\dot{i} \tag{12}$$

To realize different currents and current derivatives a trapezoidal current trajectory with different amplitudes and frequencies are used. The resulting voltage is measured and used to identify the needed parameters using a least squares approach (see Figure 8).

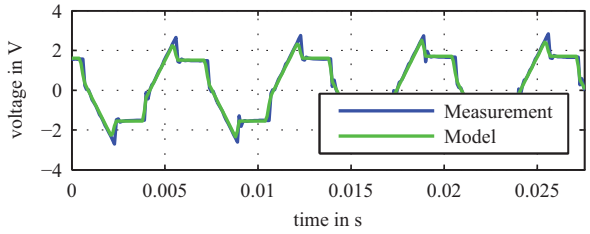

Fig. 8. Measured vs. model voltage

2) Voltage-forming constant: In order to identify the voltage-forming constant the motor current i is set to zero and thus voltage equation (2) is simplified to:

$$u = k_{\mathrm{b}} \dot{\varphi} \tag{13}$$

Equation (13) depends only on the velocity of the DC-motor $\dot{\varphi}$. Hence the DC-motor is actuated with a constant velocity by the test bed motor. Every pair of voltage u and corresponding angular velocity $\dot{\varphi}$ represents a point in Figure 9. Through all these points a straight line is fitted by least square criterion, where the slope equals the voltage-forming constant k_{b}.

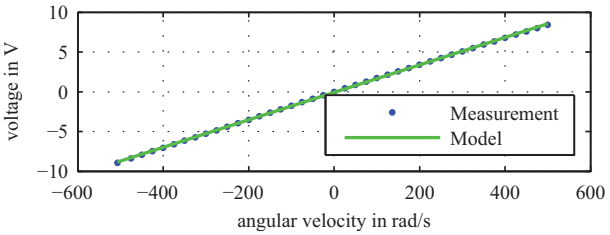

Fig. 9. Induced voltage depending on velocity

3) Eddy current constant and magnetic hysteresis constant: The effects caused by eddy current and magnetic hysteresis cannot be separated from other voltage effects, since they depend on motor current i and motor velocity $\dot{\varphi}$ (see equation (14)).

$$u = Ri + L\dot{i} + k_{\mathrm{b}}\dot{\varphi} + k_{\mathrm{EC}}\dot{\varphi}^2 i + k_{\mathrm{Hys}}\dot{\varphi} i \tag{14}$$

Thus measured voltage is corrected by the voltage of R, L and k_{b}. For identification the DC-motor was driven by the test bed motor and admitted with different currents i. The velocity and current depending corrected motor voltage is shown in Figure 10.

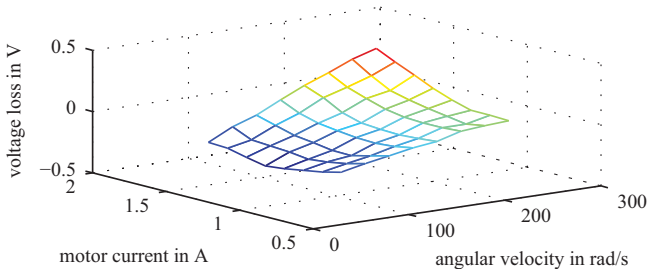

Fig. 10. Velocity and current depending voltage loss

The parameters k_{EC} and k_{Hys} are optimized with linear regression in order to fit the corrected voltage field.

B. Electromechanic Model

The most electromechanic parameters are identified at the motor test bed. One disadvantage of the motor test bed is that all measurements are affected by the additional unknown friction torque. This has to be minded and corrected while identification. Hence friction parameters are identified at the friction test bed, which is specially designed for friction identification.

1) Rotatory inertia: Without external force a mass moves uniformly. For rotatory acceleration $\ddot{\varphi}$ a torque M is needed and depends on its rotatory inertia J. In this case like in most real systems the maximum velocity is limited and hence the system has to be accelerated and decelerated alternately. As mentioned above friction distorts the measurement. To have mostly linear an correctable friction behavior, velocity $\dot{\varphi}$ has to be tall enough and not change its algebraic sign. A trajectory which satisfies all needed properties is a trapezoidal velocity trajectory with offset. Under this assumptions torque equation (7) reduces to inertia and simple friction like:

$$-M_{\mathrm{L}} = (J_{\mathrm{M}} + J_{\mathrm{T}})\,\ddot{\varphi} + \bar{\sigma}_2\dot{\varphi} + M_{\Delta} \tag{15}$$

It can be seen that the concentrated inertia of the test bed J_{T} and motor J_{M} is identified. Both inertias have to be identified separately. The test bed inertia is identified first without motor and afterwards the overall inertia is corrected by J_{T} to get the motor inertia J_{M}.

The resulting torque is measured (see Figure 11) and used to identify the parameters using the linear regression.

2) Torque-forming constant: For identification of the torque-forming constant the DC-motor is fixed in position. Under this condition all other torque components equal zero or are constant (see equation(16)).

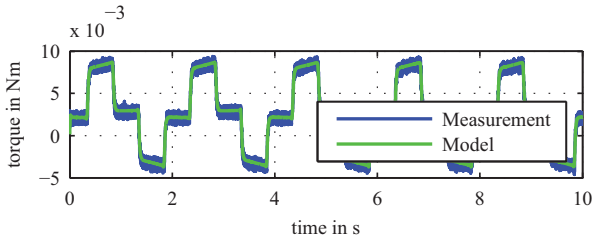

Fig. 11. Torque trajectory acceleration changes

$$-M_{\mathrm{L}} = k_{\mathrm{t}} i + M_{\Delta} \tag{16}$$

As seen in equation (16) the measured torque depends only on the motor current i and an offset torque M_{Δ}, which covers effects like cogging or friction. The motor current is set to different levels stepwise. Every step of current i produces a torque M_{L} and creates a point in Figure 12. Through all these measured points a straight line is fitted by least square criterion, where the slope equals the torque-forming constant k_{t}.

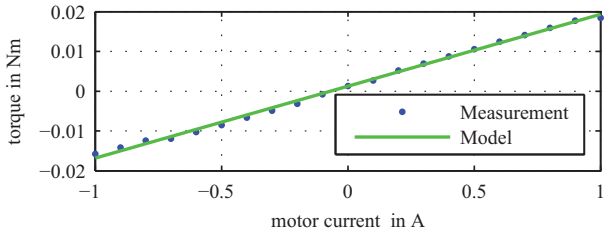

Fig. 12. Torque depending on motor current

3) Cogging Torque: The cogging torque only depends on position of the DC-motor φ. So the motor is driven with a constant velocity by the test bed motor and the current is set to zero. All other torque components equal zero or are constant under this condition and will be combined to offset torque M_{Δ}. Caused by tolerances in the production there is a small unbalance in the test bed. This produces an additional periodical torque with an frequency of one per rotation (see equation (17)).

$$-M_{\mathrm{L}} = \hat{M}_{\mathrm{Cog}} f(\varphi) + \hat{M}_{\mathrm{Un}} g(\varphi) + M_{\Delta} \tag{17}$$

All parameters are identified with the nonlinear optimization methods. Model, unbalance and measurement torque are presented in Figure 13.

4) Friction Torque: Identification of the friction parameters is performed at the friction test bed due to the friction optimized construction. Benefit of division in elastic and plastic friction domain by break away is already shown in [8] and furthermore will be used in the following identification procedure.

a) Plastic Range: The plastic friction range is dominated by the Stribeck curve, which describes the connection between

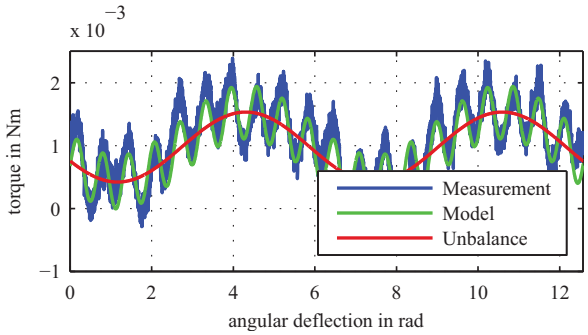

Fig. 13. Cogging torque and unbalance torque

frictional torque and velocity. In order to determine the parameters the system is driven a defined range of angles with constant velocity. Due to the fact that the acceleration equals to zero, it can be assumed that the motor torque is equal to the frictional torque.

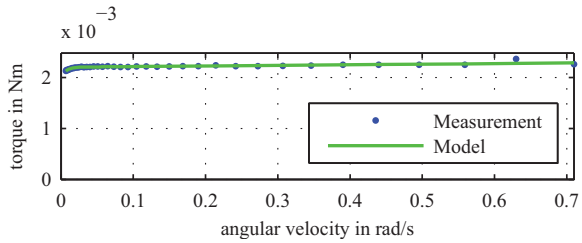

Fig. 14. Stribeck curve

The velocity and the corresponding motor torque represent one point of the Stribeck curve. Iteration for a finite number of velocities leads to the measured Stribeck curve (see Figure 14). Based on this experimental data the model parameters were identified using non-linear optimization techniques.

b) Elastic Range: This range of pure elastic friction is defined by spring-damping behavior of the bristle. A harmonic excitation induces angular deflection as well as an angular velocity profile by keeping the acceleration small. With help of linear optimization the desired parameters are determined (see Figure 15).

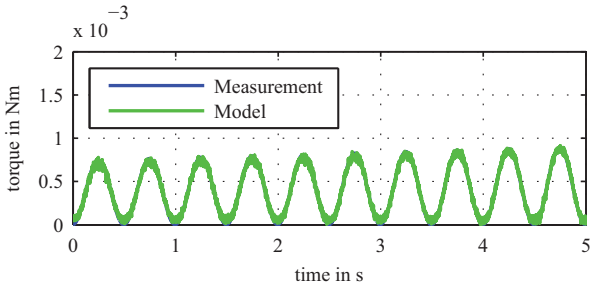

Fig. 15. Friction torque trajectories in elastic range

V. Validation

To investigate the validity and quality of the identified model, it is validated in additional experiments. Therefore, two experiments are applied to the identified model as well as the real system. The different experiments cover the effects of electromechanic model part as well as of electromagnetic model part. The used test trajectory can be seen in Figure 16 and consists of an acceleration phase with constant low and high velocity sections.

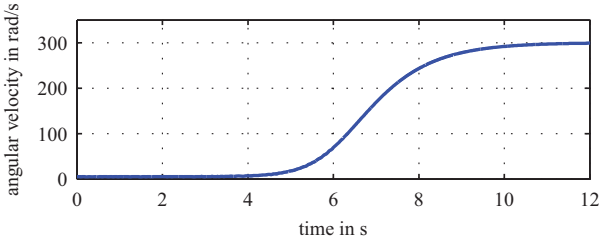

Fig. 16. Measurement trajectory for validation

To judge the quality of identification the *Normalized Root Mean Square Error (NRMSE)* is utilized.

$$NRMSE = \frac{\sqrt{\sum_{k=1}^{N} \left(x_{\text{ref}}(k) - x(k)\right)^2 / N}}{x_{\max} - x_{\min}} \times 100\% \quad (18)$$

A. Electromagnetic Model

In order to validate the electromagnetic model (see equation (2)) the DC-motor operates as engine in velocity controlled mode. In this case several values for motor current i and angular velocity $\dot{\varphi}$ are realized to cover the entire working range of the motor. For validation the presented full model and a simplified model are analyzed. The full model contains all discussed elements, whereas the simplified model is reduced by eddy current and magnetic hysteresis components.

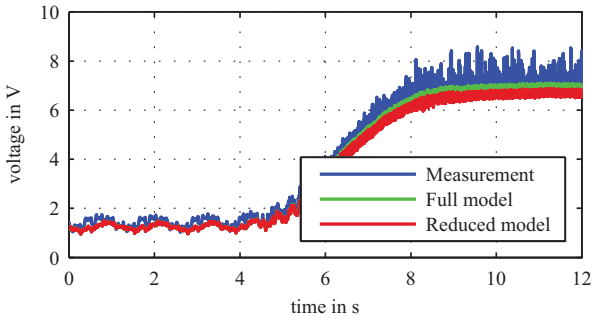

Fig. 17. Result for validation of electromagnetic model

Figure 17 shows the calculated voltage of both models and the measured voltage. It can be seen, that both models reproduce the real behavior very well for low velocities. For higher velocities, where eddy current and hysteresis losses become more important, the full model reproduces the real behavior better. The high noise on voltage measurement at high velocity is caused by commutation. Neglecting this noise the consistency of reality and both models are very good. The calculated error of both models is shown in table I.

B. Electromechanic Model

For validating the electromechanic model part (see equation (7)) the DC-motor operates as generator and is driven by the test bed motor. Here also a full and a simplified model are tested. In this case the reduced model do not includes the cogging torque. Friction torque is also modified in both models trough additional friction of the motor test bed. Validation of friction parameters was already shown in [16].

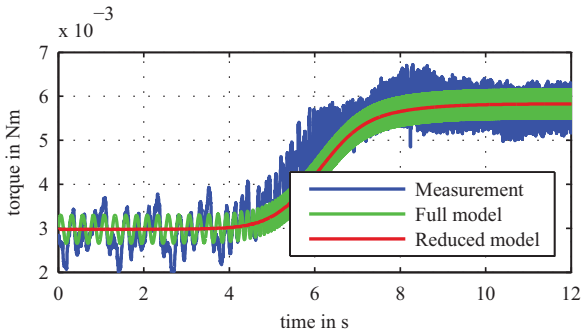

Fig. 18. Result for validation of electromechanic model

The comparison between the measurement and both models can be seen in Figure 17. The short time average of both models fits very well. Especially at low velocities the model including cogging torque reproduces the measurement even better. Caused by the disturbance, e.g. of test bed unbalance, this improvement is not obvious in the model error (see Table I).

TABLE I
NRMSE FOR MOTOR MODEL

Model	Typ	NRMSE
electromechanic model	full	8.56%
electromechanic model	reduced	8.68%
electromagnetic model	full	4.57%
electromagnetic model	reduced	5.99%

It could be shown that the identified parameters give very good connection to their real equivalents and the extended DC-motor model represents excellent the whole range of system behavior.

VI. CONCLUSION

This work presents an extended model for permanent magnet direct current motors besides associated parameter identification. Starting with a survey of electromagnetic and electromechanic phenomena, a motor model was developed. In equivalent to observation in reality the model was extended by electromechanic effects like cogging and friction, and electromagnetic effects generated by eddy current and magnetic hysteresis. These effects were synthesized on their theoretical principles and summarized to investigable parameters in reality. After that, model parameters were determined in specialized experiments at two proprietary developed high precision test benches. According to modeling and identification the DC-motor model was validated in separate experiments. For the electromagnetic as well as for the electromechanic part a full and a reduced model were validated. The full model contains all modeled components, while the reduced models were shortened by eddy currents and magnetic hysteresis and cogging effects respectively. It can be seen, that the identified parameters a show very good relation to the real behavior. The extended full models fit reality even better.

ACKNOWLEDGMENT

The work was supported by the IAV GmbH. The authors would also like to thank all colleagues at IAV GmbH and Ilmenau University of Technology who have contributed to the developments described.

REFERENCES

[1] G. Müller, K. Vogt, and B. Ponick, *Berechnung elektrischer Maschinen*. Wiley-VCH Verlag, 2008.
[2] W. Wu, "Dc motor identification using speed step responses," in *IEEE American Control Conference*, 2010.
[3] X.-Q. Liu, H.-Y. Zhang, J. Liu, and J. Yang, "Fault detection and diagnosis of permanent-magnet dc motor based on parameter estimation and neural network," in *IEEE Transactions on Industrial Electronics*, vol. 47, no. 5, 2000.
[4] J. Gros, G. C. R. Sincero, and P. Viarouge, "Design method for brush permanent magnet dc motors," in *IEEE Electric Machines and Drives Conference*, 2009, pp. 1625 – 1632.
[5] A. Amthor, S. Zschaeck, and C. Ament, "High precision position control using an adaptive friction compensation approach," *Automatic Control, IEEE Transactions on*, vol. 55, no. 1, pp. 274 – 278, Jan. 2010.
[6] S. Zschaeck, A. Amthor, and C. Ament, "Decentralized high precision motion control for nanopositioning and nanomeasuring machines," in *IECON 2011 - 37th Annual Conference on IEEE Industrial Electronics Society*, Nov. 2011, pp. 546 –551.
[7] P. Dupont, V. Hayward, B. Armstrong, and F. Altpeter, "Single state elasto-plastic friction models," *Automatic Control, IEEE Transactions on*, vol. 47, no. 5, pp. 787 –792, May 2002.
[8] S. Buechner, S. Zschaeck, A. Amthor, C. Ament, and M. Eichhorn, "Dynamic friction modeling and identification for high precision mechatronic systems," in *IECON 2012 - 38th Annual Conference on IEEE Industrial Electronics Society*, 2012, pp. 2263–2268.
[9] C. C. De Wit, H. Olsson, K. J. Aström, and P. Lischinsky, "A new model for control of systems with friction," *IEEE Trans. Autom. Control*, vol. 40, no. 3, pp. 419–425, Mar. 1995.
[10] B. Armstrong-Héouvry, P. Dupont, and C. De Wit, "A survey of Models, Analysis Tools and Compensation Methods for Control of Machines with Friction," *Automatica*, vol. 30(7), pp. 1083–1138, 1994.
[11] C. Bretón, J. Bartolomé, A. Benito, G. Tassinario, I. Flotats, C. W. Lu, and B. J. Chalmers, "Influence of machine symmetry on reduction of cogging torque in permanent-magnet brushless motors," in *IEEE Transactions on Magnetics*, vol. 36, no. 5, 2000.
[12] Y. Yang, X. Wang, C. Zhu, and C. Huang, "Study of magnet asymmetry for reduction of cogging torque in permanent magnet motors," in *IEEE Industrial Electronics and Applications*, 2009.
[13] dSpace GmbH. [Online]. Available: http://www.dspace.de/
[14] Dr. Johannes Heidenhain GmbH. [Online]. Available: http://www.heidenhain.de/
[15] Kistler Instrumente AG. [Online]. Available: http://http://www.kistler.com/
[16] S. Buechner, A. Amthor, S. Zschaeck, C. Ament, and M. Eichhorn, "Dynamic friction modeling for dc-motors," in *Automotive Powertrain Control Systems*, 2012, pp. 119–128.